

## Supporting Information for

### **Atomic Scale Interfacial Transport at an Extended Evaporating Meniscus**

Yigit Akkus<sup>a,b</sup>, Anil Koklu<sup>a</sup>, Ali Beskok<sup>a</sup>

<sup>a</sup>Lyle School of Engineering, Southern Methodist University, Dallas, TX 75205, USA

<sup>b</sup>ASELSAN Inc., 06172 Yenimahalle, Ankara, Turkey

- A. Details of molecular dynamics simulations
- B. Mass flow through adsorbed region
- C. Uncertainty analysis
- D. Location and profile of evaporating meniscus for different heating loads
- E. Flow and temperature fields

## A. Molecular dynamics simulations

Two systems are simulated. Except the number of fluid (Ar) atoms and the interaction between fluid and solid atoms, both systems are identical and subjected to same computational procedure. Systems have identical channel walls composed of (3240x2=6480) Platinum (Pt) atoms. Each wall has 4 solid layers and (1,0,0) crystal planes facing the liquid. The outermost layer of the walls is always fixed at their lattice positions. 4200 and 5775 fluid atoms are used in the first and second simulations, respectively. Numbers of fluid atoms are selected such that condensed phase is always attached to the channel inlets and outlets and the effective radius of curvature (based on a circular fit) at the interface is approximately the same for both systems, when the systems are isothermally equilibrated before the initiation of the heating/cooling process. Periodic boundary conditions are applied in all directions. Time step is 5 fs and each collected data is averaged for 2 ns. Lennard-Jones (L-J) 6-12 potential is used to model the interactions between Ar-Ar and Ar-Pt atoms with molecular diameters of  $\sigma_{\text{Ar}} = 0.34$  nm,  $\sigma_{\text{Ar-Pt}} = 0.3085$  nm, and depth of the potential wells of  $\epsilon_{\text{Ar}} = 0.01042$  eV,  $\epsilon_{\text{Ar-Pt}} = 0.00558$  eV for the first and  $\epsilon_{\text{Ar-Pt}} = 0.0558$  for the second simulation [S. Maruyama and T. Kimura, *Therm. Sci. Eng.* **7** (1999)]. L-J potential is truncated with a cut-off distance of  $3\sigma_{\text{Ar}}$ . Embedded atom model is utilized for Pt-Pt atomic interactions [32]. Simulations are started from the Maxwell-Boltzmann velocity distribution for all atoms at 110 K. Nosé-Hoover thermostat is applied to all atoms (except the outermost Pt layers) for 15 ns to stabilize the system temperature at 110 K. Then, microcanonical ensemble is applied to Ar atoms for 15 ns to equilibrate the system, while solid atoms are still subjected to the thermostat. At the end of the isothermal stage, stable liquid/vapor Ar mixture is attained at 110 K. Then, equal energy injection/extraction (first simulation:  $\dot{q}=11$  nW, second simulation:  $\dot{q}=20$  nW) is applied to the wall atoms located at the heating/cooling zones for 40 ns. Other wall atoms are not allowed to vibrate in order to eliminate heat conduction through the solid wall. Average temperatures of the solid wall atoms in heating/cooling zones for the first and second simulations are  $177.10 \pm 1.94$  K /  $76.97 \pm 0.71$  K and  $173.60 \pm 2.64$  K /  $78.97 \pm 0.55$  K, respectively. During heating/cooling, fluid atoms are subjected to microcanonical ensemble. At the end of heating/cooling period, statistically stable phase changing liquid/vapor interfaces are formed at both ends of the channel. The rates of the steady passive liquid flow from condensing interface to evaporating interface through the channel are calculated as ‘ $743.6 \pm 15.2$  #<sub>Ar</sub>/ns’ and ‘ $504.4 \pm 12.1$  #<sub>Ar</sub>/ns’ for the first and second simulations, respectively. As an experimental observation [33,34], molecular layering of fluid near a solid should be considered as a link to the real-world behavior of the system. During all simulations, molecular layering of Ar is verified in the proximity of the walls. Moreover, the distribution and magnitude of the density peaks are in good agreement with the results of [S. Maruyama and T. Kimura, *Therm. Sci. Eng.* **7** (1999)], where same L-J potential parameters were used. All simulations are carried out using Large-scale Atomic/Molecular Massively Parallel Simulator (LAMMPS) [S. Plimpton, *J. Comput. Phys.* **117** (1995)].

## B. Mass flow through adsorbed region

Mass flow rate through a cross section area,  $A$ , is functions of density,  $\rho$ , and velocity,  $\vec{u}$  :

$$\dot{m} = \int (\rho \vec{u}) \cdot \vec{n} dA \quad (1)$$

where  $\vec{n}$  is the unit normal vector of the surface, across which the mass flow is calculated. Within the adsorbed layer, mass flow rate along the surface coordinate ‘s’ can be expressed per unit channel depth as follows:

$$\dot{m}'|_s = \int_0^{\delta^*} (\rho \vec{u}) \cdot \vec{n} d\delta \quad (2)$$

where  $\delta$  is the coordinate along the surface normal and  $\delta^*$  is the thickness of the adsorbed layer. Mass flow rate at a specific ‘s’ location can be calculated by approximating the above equation using rectangle rule of numerical integration, which requires summing the mass flow rates through the bins positioned at this ‘s’ location (see Figure S1).

$$\dot{m}'|_s = \left( b \sum_i (\rho \vec{u})_i \right) \cdot \vec{n} \quad (3)$$

where  $b$  is the height of each bin. When the velocity vector ( $\vec{u} = u\vec{i} + v\vec{j}$ ) and the unit normal vector ( $\vec{n} = n_x\vec{i} + n_y\vec{j}$ ) are decomposed to its components in horizontal and vertical directions, equation (3) can be expressed in terms of the contributions of mass flow rate in the horizontal and vertical directions as follows:

$$\dot{m}'|_s = b \sum_i [(\rho u)_i n_x + (\rho v)_i n_y] \quad (4)$$

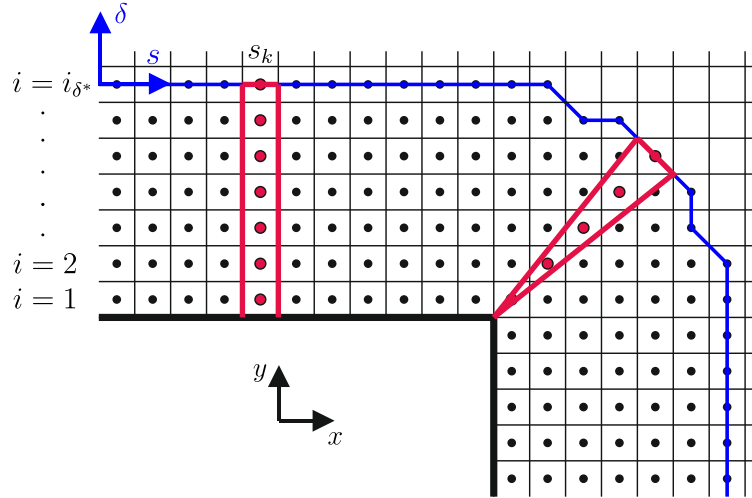


**Figure S1:** Mass flow calculation through adsorbed region. The figure is plotted for demonstration purposes and it does not reflect the real adsorbed layers observed in simulations, which contain much higher number of bins. The dots show the center of each bin, where the flow properties are averaged in time. Blue line shows the liquid/vapor interface, which is formed by connecting the center of bins having higher density than the cut-off density (see Supplemental Material 2). Mass flow is calculated along this interface, *i.e.* along the surface coordinate ‘s’. Step size (arc length of interface at each step) is determined by connecting the mid points of two successive bin centers. Mass flow rate at each step is calculated by summing the mass flow rates of all bins located between the surface and wall. The red rectangle and the red dots within this region show contributing bins to the mass flow calculated at a certain step along the inner wall surface. The red triangle, on the other hand, specifies the contributing bins at a certain step at the corner region.

### C. Uncertainty analysis

Density, velocities and temperature are sampled at every 2 ns and all the data collected between the two measurements is averaged, which yields a measurement uncertainty,  $\varepsilon$ , for each time averaged data,  $\langle \dots \rangle$ .

$$\rho = \langle \rho \rangle \pm \varepsilon_\rho \quad (5a)$$

$$u = \langle u \rangle \pm \varepsilon_u \quad (5b)$$

$$v = \langle v \rangle \pm \varepsilon_v \quad (5c)$$

$$T = \langle T \rangle \pm \varepsilon_T \quad (5d)$$

Uncertainties associated with density ( $\varepsilon_\rho$ ), horizontal velocity ( $\varepsilon_u$ ), vertical velocity ( $\varepsilon_v$ ) and temperature ( $\varepsilon_T$ ) are estimated by calculating the standard error of measurements, which is evaluated by dividing the standard deviation of measurements to the number of samples.

Mass flux is simply the multiplication of density and velocity. Estimation of mass flux has also associated uncertainty due to the time averaging.

$$\rho u = \langle \rho u \rangle \pm \varepsilon_{\rho u} \quad (6a)$$

$$\rho v = \langle \rho v \rangle \pm \varepsilon_{\rho v} \quad (6b)$$

Uncertainties of mass fluxes in horizontal and vertical directions are expressed in terms of the uncertainties of density and velocities as follows:

$$\varepsilon_{\rho u} = \sqrt{(\varepsilon_\rho u)^2 + (\varepsilon_u \rho)^2} \quad (7a)$$

$$\varepsilon_{\rho v} = \sqrt{(\varepsilon_\rho v)^2 + (\varepsilon_v \rho)^2} \quad (7b)$$

Mass flow rate through surface coordinate 's' is calculated using equation (4), where the mass flow rate under a specific surface coordinate 's' is the summation of horizontal and vertical mass fluxes through each bin positioned at the 's' location. Therefore, uncertainty of the mass flow rate depends on the uncertainties of mass fluxes at the contributing bins as shown in equation (8).

$$\dot{m}'|_s = b \left\langle \sum_i [(\rho u)_i n_x + (\rho v)_i n_y] \right\rangle \pm b \sqrt{\sum_i [(\varepsilon_{\rho u})_i n_x]^2 + [(\varepsilon_{\rho v})_i n_y]^2} \quad (8)$$

When equation (7) is inserted into equation (8), mass flow rate and its uncertainty can be expressed as the functions of the measured data and their measurement uncertainties as follows:

$$\dot{m}'_s = b \left( \sum_i [(\rho u)_i n_x + (\rho v)_i n_y] \right) \pm b \sqrt{\sum_i [(\varepsilon_{\rho u})_i^2 + (\varepsilon_{u\rho})_i^2] (n_x)^2 + [(\varepsilon_{\rho v})_i^2 + (\varepsilon_{v\rho})_i^2] (n_y)^2} \quad (9)$$

#### D. Location and profile of evaporating meniscus for different heating loads

Before heating, the system was isothermal and already equilibrated. Number of fluid atoms is selected such that liquid is attached to the channel inlets prior to heating. During simulations, different heating rates ( $\dot{q}$ ) are applied to observe the response of evaporating meniscus. As shown in Figure S2, heating rates above 6 nW yield apparent meniscus deformations. Between 6 nW and 9 nW, evaporative mass flux increases more than 50% in the expense of a 10 K superheat rise. However, after 10 nW, mass flux slightly increases, whereas the superheat elevates more than 10 K. To explain this behavior, morphology of the liquid/vapor interface is examined at the each heating rate. Between 6 nW and 9 nW, liquid meniscus was attached to the channel inlets. However, after 10 nW, the extended meniscus is detached from the channel tips and receded into channel. During the simulation with 12 nW heating, evaporation resistance experienced a jump, which is accepted as the indication of burnout and the simulation is ceased. Second order curve fittings (red dashed curves) applied to these data groups and two different regimes (pinning and receding) are identified. This regime shift were previously demonstrated by a recent study [35], where the minimum nanopore modeled had a hydraulic diameter of 20 nm.

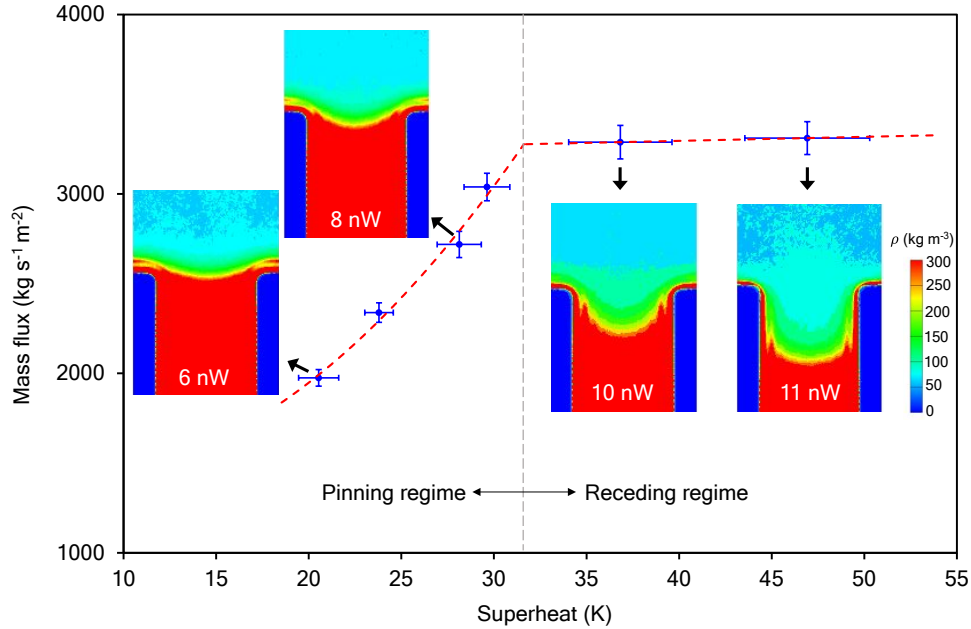


**Figure S2:** Evaporative mass flux vs. superheat for the first simulation together with the location and profile of evaporating meniscus at different heating rates.

#### E. Flow and temperature fields

Flow and temperature fields near the evaporating interface are provided in Figure S3:

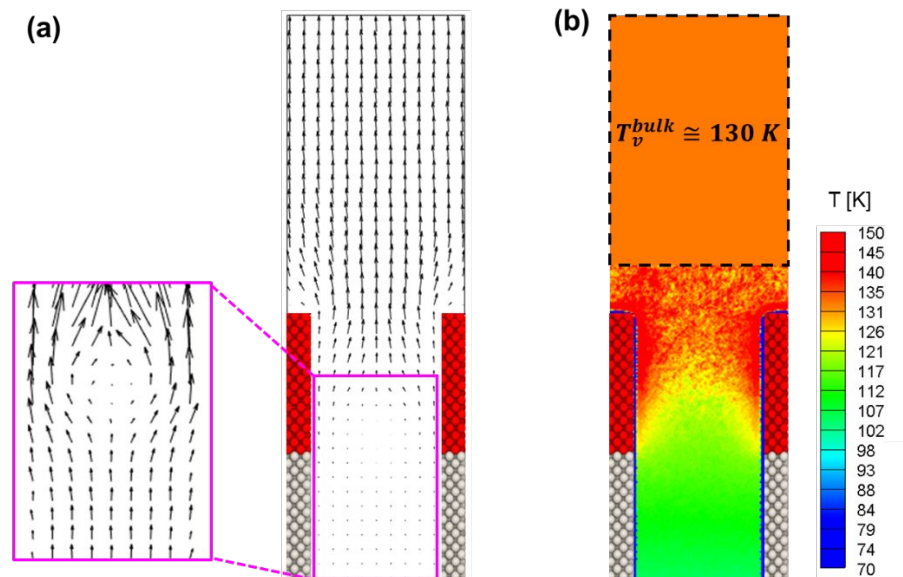


**Figure S3:** (a) Velocity vectors for fluid flow. Inset shows the velocity vectors close to the evaporating meniscus, where magnitude of the vectors is 10 times increased. (b) Temperature field near the evaporating interface. While smaller sized bins are utilized in the close vicinity of the interface and liquid phase, a large bin is used to calculate the temperature of the bulk vapor phase.

In the gas phase, higher velocities are depicted as expected, and, away from the interfaces, gas velocity is almost constant. Liquid velocities, on the other hand, are comparatively low and their magnitudes are additionally reported in the inset by enlarging their vector sizes to enable the detection of velocity variation between the walls.

The effect of heating on fluid atoms is prominent near the heated (red) wall atoms. Narrow blue region adjacent to the wall is the gap region formed by the repulsion between fluid and wall atoms, and, there is no temperature data for this gap due to the absence of atoms in this region. In order to capture the variation of temperature with a high spatial resolution, small sized bins are utilized during data sampling for the temperature. Although temperature of the condensed phase can be precisely calculated using these small bins, a spotted distribution of the temperature forms in the gas phase due to the insufficient number of atoms passing through the bin in a certain time interval. When the bin size is increased, in other words, when more atoms are included during the calculation of the temperature in each single bin, an almost constant temperature ( $130.0 \pm 1.5$  K) is achieved in the bulk gas region above the evaporating interface.